Journal of Hydrology 589 (2020) 125154

Contents lists available at ScienceDirect

Journal of Hydrology

journal homepage: www.elsevier.com/locate/jhydrol

Research papers

Quantifying the effects of urbanization on floods in a changing environment to promote water security — A case study of two adjacent basins in Texas☆

Manqing Shao[a], Gang Zhao[a], Shih-Chieh Kao[b], Lan Cuo[c,d], Cheryl Rankin[a], Huilin Gao[a,*]

[a] Zachry Department of Civil and Environmental Engineering, Texas A&M University, College Station, TX 77843, United States
[b] Environmental Sciences Division and Climate Change Science Institute, Oak Ridge National Laboratory, Oak Ridge, TN 37831, United States
[c] Key Laboratory of Tibetan Environment Changes and Land Surface Processes, Institute of Tibetan Plateau Research, Center for Excellence in Tibetan Plateau Earth Sciences, Chinese Academy of Sciences, Beijing 100101, China
[d] University of Chinese Academy of Sciences, Beijing 100101, China

ARTICLE INFO

Keywords:
Urbanization
Paired catchments
Hydrological modeling
Changing climate
Land cover change
Water security

ABSTRACT

The increased occurrence of flood events resulting from urbanization and global climate change is a great threat to water security. To systematically evaluate the impacts of urbanization on floods, we applied a *paired catchments* approach to two adjacent river basins in south-central Texas — the San Antonio River Basin (SARB), with fast urbanization; and the Guadalupe River Basin (GRB), with little land cover change. A physics-based distributed hydrological model — the Distributed Hydrology Soil Vegetation Model, embedded with a multi-purpose reservoir module (DHSVM-Res) — was used to simulate streamflow and reservoir storage. The simulations were conducted under different land cover scenarios, including a newly developed continuous land cover series (CLCS). Holistic analyses were then conducted for the paired basins using three methods: analyzing the selected flood events, detecting change points (CP) of monthly floods, and testing the elasticity of long-term flood regimes. The results suggest that: (1) urbanization may reduce lag time and elevate flood peaks significantly by 3–30% in our study area; (2) when there is little land cover change, changing climate is the major driver of variations in the monthly maximum streamflow (MMS); (3) fast urbanization can amplify streamflow variability, increase MMS significantly, and thus alter the timing of CP; and (4) the mean MMS of observed streamflow in the SARB has increased by as much as 75.7% from the pre-CP to post-CP periods. This comprehensive study fills in a gap in our current understanding of the isolated impacts of urbanization on flooding and is expected to support future explorations of anthropogenic influences on floods.

1. Introduction

Global urbanization exacerbates the negative socioeconomic impacts from severe climatic disasters (e.g., floods and droughts) (United Nations, 2009, 2011; Jha et al., 2012). For example, urbanization is associated with increasing impervious area and decreasing infiltration, which can lead to more frequent and severe flooding (Cuo, 2016; DeFries and Eshleman, 2004; Jongman, 2018; Nowak and Greenfield, 2012; OniStephen et al., 2015). This directly endangers our societal safety as well as infrastructure stability (Jha et al., 2012), which threatens water security and hinders improvements in water related infrastructure (Hall and Borgomeo, 2013; Gain et al., 2016; Yangon, 2016). Thus, it is critical for policymakers to update water management plans and promote water security through evaluating the influence of urbanization on floods (Winters et al., 2015; Cross et al., 2018; Emmett et al., 2018).

In recent decades, the frequency and intensity of various climate extremes have increased substantially (Alexander et al., 2006; Zhang et al., 2011; Donat et al., 2013). For example, in the United States, nine of the top ten most extreme 1-day precipitation events from 1910 to 2015 occurred after 1990 (NOAA, 2019). This intensification of heavy precipitation has also been observed in other parts of the world, such as

☆ This manuscript has been co-authored by an employee of Oak Ridge National Laboratory, managed by UT Battelle, LLC, under contract DE-AC05-00OR22725 with the U.S. Department of Energy. The United States Government retains and the publisher, by accepting the article for publication, acknowledges that the United States Government retains a non-exclusive, paid-up, irrevocable, world-wide license to publish or reproduce the published form of this manuscript, or allow others to do so, for United States Government purposes. The Department of Energy will provide public access to these results of federally sponsored research in accordance with the DOE Public Access Plan (http://energy.gov/downloads/doe-public-access-plan).

* Corresponding author at: Department of Civil and Environmental Engineering, Texas A&M University, College Station, TX 77843, United States.
E-mail address: hgao@civil.tamu.edu (H. Gao).

https://doi.org/10.1016/j.jhydrol.2020.125154

Available online 06 June 2020

the United Kingdom, South Africa, India, and Japan (Groisman et al., 2005; Goswami et al., 2006; Min et al., 2011; Westra et al., 2013; Kunkel & Frankson, 2015; Donat et al., 2016). Some regions have shorter, more intense storms compared to other regions, which leads to unexpected severe floods. Recently, the Hurricane Harvey event (August 25 – 31, 2017) — which was ranked as the second most destructive storm in U.S. history (Hurricane Katrina being the worst, in inflation-adjusted costs of $161 billion) (Natsios, 2019) — resulted in damages of around $125 billion. Combined with other factors such as urbanization, the impacts from intensified climate extremes can be further non-linearly enhanced. Thus, it is important to understand the mechanism of the hydrological changes under these impacts.

However, while it is imperative to evaluate the distinct impacts of urbanization and the changing climate on flooding to better support decision making (in terms of flood control and urban planning), such effects are challenging to quantify separately. Since both climate and land cover affect streamflow, it is difficult to separate their effects when a single basin is investigated. Thus, neighboring basins with similar physical characteristics (e.g., climate pattern, topography, soil texture, vegetation)—but different paces of urbanization—are ideal study areas that can be used to isolate the land cover impacts and the climate impacts.

One of the most common practices used to separate the effects of urbanization and climate is *paired catchments* analysis (Ochoa-Tocachi et al., 2016; Seibert and McDonnell, 2010; Zhao et al., 2010). The *paired catchments* study originated from a forestry study (Bates & Henry, 1928) and has since been widely used to evaluate the influences of changes in land cover on the magnitudes of water yields (Bosch and Hewlett, 1982; Brown et al., 2005; Ide et al., 2013; Schelker et al., 2013). In recent years, this method has also been applied to investigate the effects of urbanization on streamflows (Burns et al., 2005; OniStephen et al., 2015; Putro et al., 2016; Zégre et al., 2010). Typically, a “reference basin” and an “urbanized basin”—with similar physical characteristics—are selected to isolate the effects of urbanization. Regression models or conceptual frameworks are usually applied to analyze the results from the paired river basins (Burns et al., 2005; Zhao et al., 2010a). While this approach provides a systematic way to disentangle the combined issues, other anthropogenic factors (e.g., reservoir regulation and irrigation schemes) may further complicate the analysis and hamper an accurate quantification (Zégre et al., 2010). Hence, it is necessary to use additional tools and methods to further extract the influence of urbanization on flooding when studying the *paired catchments*.

Unlike lumped models, distributed physics-based models can be employed to represent the spatial heterogeneity of the soil and vegetation parameters, and the meteorological forcing data (Giertz et al., 2006). Such models have a distinct advantage of being able to simulate streamflow under various land use/cover change (LUCC) scenarios at high spatial and temporal resolution (Motta & Tucci, 1984; Wigmosta et al., 1994; Brirhet & Benaabidate, 2016). For example, a 2008 study used the MIKE SHE model to study the effects of five types of land use changes on streamflow in a Korean river basin (Im et al., 2008). Cuo et al. (2008) employed the Distributed Hydrology Soil Vegetation Model (DHSVM) to study the effects of continuing urbanization on peak flows in a partially urbanized basin in the State of Washington. Zhao et al. (2016a) compared DHSVM simulations under different historical and projected land-cover maps in Texas’s San Antonio River Basin and found that urbanization alone had a profound impact on the increased peak streamflow. With the availability of coupled hydrologic and reservoir management models (e.g., DHSVM-Res; Zhao et al., 2016b), distributed models can be further used to study areas under significant reservoir regulation that cannot be addressed through conventional, natural, ‘streamflow-only’ models.

In addition to the above approaches, using detrended climate data coupled with a series of LUCC snapshots in time is a commonly adopted modeling approach used to isolate the effects of LUCC and climate change/variability on streamflow. For example, detrended daily rainfall was used in the Variable Infiltration Capacity (VIC) hydrological model to evaluate the relative impacts of climate and land cover changes in the Godavari River Basin, India (Hengade and Eldho, 2019). In the Andean basins of South America, precipitation and streamflow time series datasets which were influenced by the El Niño–Southern Oscillation, were detrended to disentangle the impacts of climate variability and LUCC (Molina et al., 2015). However, in these types of studies, the results can be easily affected by the uncertainties associated with the selection of the time period. Overall, our current understanding about the isolated influence of urbanization on floods is limited because of two main obstacles: the joint effects of urbanization and changing climate are difficult to distinguish, and other human-induced factors such as reservoir regulation also plays a role (Kaushal et al., 2008; Hejazi Mohamad & Markus, 2009).

With an overarching goal of improving water security, our specific objective in this study is to systematically evaluate the impacts of urbanization on flooding by leveraging both *paired catchments* analysis and physics-based distributed hydrological modeling with an embedded multi-purpose reservoir module. Specifically, DHSVM-Res was selected to simulate the hydrological processes due to its explicit urban and reservoir modules, and its high spatial and temporal resolutions. Two adjacent Texas river basins — one with little LUCC and one with considerable urbanization — are compared holistically via a stepwise methodology. First, the flood characteristics (e.g., peak flow and peak time) of several observed/simulated flood events are analyzed for the paired basins. Second, changes in the monthly flood-related variables are studied via a change point detection method (Killick & Eckley, 2014). Third, a newly defined elasticity test is conducted to evaluate the sensitivity of the flood peak flows to different urban land cover conditions under perturbed precipitation conditions.

2. Study area

Texas is the largest state in the contiguous United States (CONUS), and its climate is characterized by drastic spatial and temporal variations throughout the state (Kottek et al., 2006). Two adjacent river basins in south-central Texas — the San Antonio River Basin (SARB), and the Guadalupe River Basin (GRB) — are selected as the study area (Fig. 1). The San Antonio River merges into the Guadalupe River about 16 km upstream of San Antonio Bay (located adjacent to the Gulf of Mexico). Both basins have similar precipitation climatology (Fig. 2a), vegetation types (e.g., grass and shrub), and soil types (e.g., clay). The characteristics of the paired basins are further compared in Fig. S1 and Table S1 (Supplementary Material). Both basins are vulnerable to recurring tropical storms (including hurricanes) due to their geographical proximity to the Gulf Coast (Guannel et al., 2010).

The SARB has a drainage area of 10,826 km^2. The elevation of the basin ranges from 4 m to 693 m above sea level, and the average annual precipitation was 813 mm from 1966 to 2011(Livneh et al., 2013). There are six subbasins in the SARB: the Medina River, the Leon Creek, the Salado Creek , the upper San Antonio River, the Cibolo Creek, and the lower San Antonio River subbasins (Fig. 1). The city of San Antonio — the second-most populous city in Texas — has experienced rapid urbanization. The urban population doubled from 0.65 million in 1970 to 1.30 million in 2010, and the impervious area almost tripled from 325 km^2 (3.0%) to 903 km^2 (8.3%) during the same period (Fig. 2b; Price et al., 2006; Jin et al., 2013; Thomas et al., 2013).

The GRB has a drainage area of 15,418 km^2. The elevation of the basin ranges from 1 m to 735 m above sea level, and the annual average rainfall was 889 mm from 1966 to 2011 (Livneh et al., 2013). The GRB consists of four subbasins: the upper Guadalupe River, the San Marcos River, the middle Guadalupe River, and the lower Guadalupe River subbasins (Fig. 1). In contrast to the SARB, the GRB only had a population of approximately 0.24 million in 1970 and approximately 0.33 million in 2010 (Thomas et al., 2013). From 1970 to 2010, the

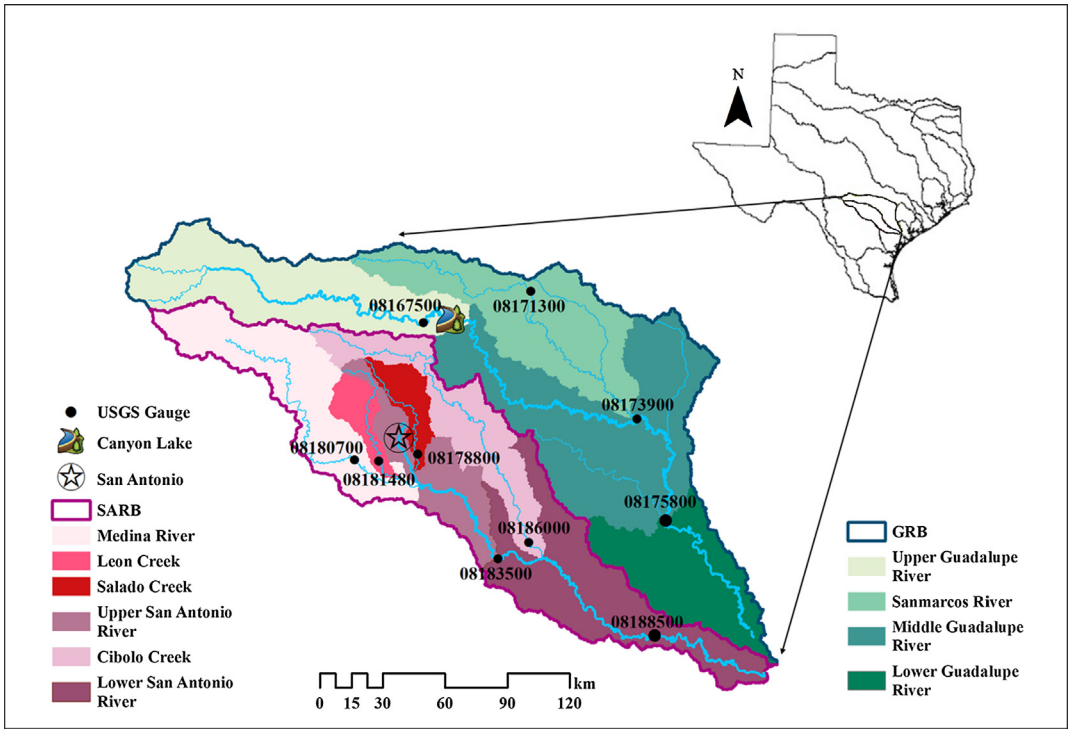

Fig. 1. Map of the study area, which includes the San Antonio River Basin (SARB) and the Guadalupe River Basin (GRB). The subbasins of each river basin are denoted in different colors.

impervious area of the GRB increased slightly from 93 km^2 (0.6%) to 132 km^2 (0.9%) (Fig. 2b; Price et al., 2006; Jin et al., 2013). There is a flood control reservoir within the GRB — Canyon Lake (29.86°N, 98.20°W; Fig. 1) — that has been operated at the conservation level since 1968 by the U.S. Army Corps of Engineers.

3. Methodology and data

3.1. Hydrological model and input data

3.1.1. Hydrological model

The Distributed Hydrology Soil Vegetation Model (Wigmosta et al., 1994), with an embedded multi-purpose reservoir module (DHSVM-Res, Zhao et al., 2016b), was used to simulate the streamflow of the SARB and GRB. DHSVM-Res is an open-source, physics-based, fully distributed model which computes the energy and water balances at each grid cell. The model can be set up at a high spatial resolution (e.g., 10 – 200 meter) and at a sub-daily time step (e.g., 1 – 24 hour), which together can facilitate the simulation of flood response. In this study, DHSVM-Res was set up at a 200-meter spatial resolution and at a 3-hourly time step from 1965 to 2011 with the first year used for model spin-up.

One of the major advantages of DHSVM-Res is its explicit urban module (Cuo et al., 2008). Coupled with the spatially distributed features of the model, the urban module can simulate the flow path from an urban pixel to its nearest river channel. For each urban pixel, the fraction of impervious area and the fraction of water stored in flood detention are both specified. The fraction of impervious area determines the amount of surface runoff which is diverted to detention storage and follows the designed detention process. Then, based on the outflow from detention, discharge to the nearest channel is calculated. With the support of this module, the spatial heterogeneity of the urban sprawl (e.g., denser urbanization along highways) can be explicitly simulated.

Another recently added feature of DHSVM is a multi-purpose (e.g., flood control, water supply) reservoir module (Zhao et al., 2016b, 2018). The reservoir module consists of three components: the evaporation scheme, the release scheme, and the storage calculation

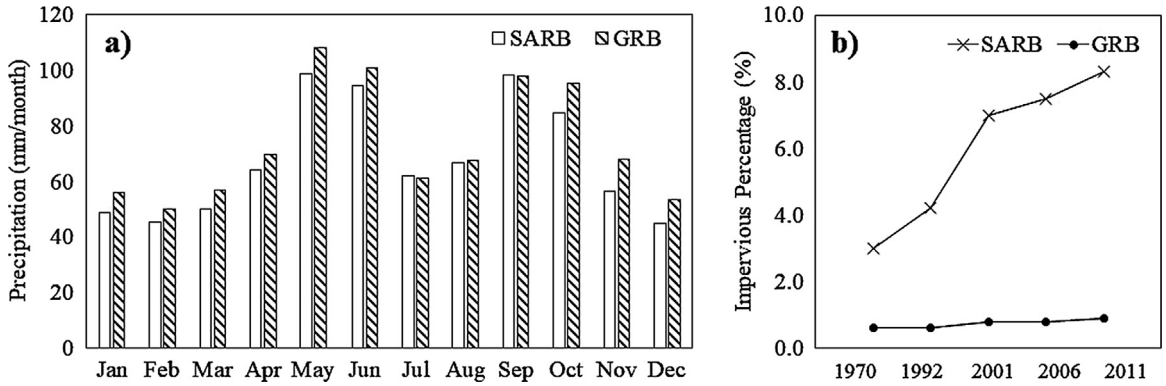

Fig. 2. a) Monthly precipitation climatology in the GRB and the SARB (1966 – 2011). Data are adopted from Livneh et al. (2013). b) The impervious percentages of the GRB and the SARB are from 1970 to 2011.

(which calculates the overall water balance of the reservoir). The reservoir releases water based on prescribed operation rules. By incorporating this module during the calibration and validation processes—and then removing its effects in the following simulation—naturalized flow can be obtained. It is a common practice to create naturalized flow. For example, in Döll et al. (2009) naturalized flow was computed by removing all reservoirs in the global water model WaterGAP simulation to quantify the impacts of reservoir regulation on streamflow. In our study, this methodology facilitates the separation of the urbanization impacts from the influences of reservoir flow regulation.

3.1.2. Input data

There are three types of input data for DHSVM-Res: land surface parameters, reservoir configurations, and meteorological forcing data.

- **Land surface parameters** include elevation, soil, and land cover data. The elevation data — Digital Elevation Model (DEM) map — was adopted from the Shuttle Radar Topography Mission 30-meter resolution product (Jarvis et al., 2008), and was resampled to 200-meter. The basin mask was created based on the DEM using ArcMap 10.3. The flow direction, the stream network, and the soil depth were generated using the DEM and python scripts from Duan (2018). Soil texture data was obtained from the Soil Survey Geographic Database (SSURGO; Nauman et al., 2018). Land cover data were collected from three sources: 1) the United States Geological Survey (USGS) National Land Cover Database (NLCD), which includes NLCD1992, NLCD2001, NLCD2006, and NLCD2011 (Vogelmann et al., 2001; Homer et al., 2007; Fry et al., 2011; Jin et al., 2013); 2) the USGS Enhanced Historical Land-Use and Land-Cover Datasets, which depict LUCC from the 1970s to 1980s (referred to as LC1970 hereinafter; Price et al., 2006); and 3) the continuous land cover series (CLCS), which depicts the continuous urban expansion of the City of San Antonio for each year from 1984 to 2011. The CLCS was generated by combining the baseline map — LC1970 — with the classified annual urban land cover maps, which were derived from annual Landsat 5 Thematic Mapper images. The steps of CLCS generation are demonstrated in Text S1 of the Supplementary Material.
- **Reservoir configurations** (storage, elevation, and surface area) for Canyon Lake (Fig. 1) were acquired from the Texas Water Development Board and were used to derive the reservoir rating curve (Fig. S5, Supplementary Material). The storage capacity of Canyon Lake (1.5×10^9 m^3) was divided by the U.S. Army Corps of Engineers into a surcharge pool (1.1×10^8 m^3), a flood control pool (9.1×10^8 m^3), a conservation pool (4.8×10^8 m^3), and an inactive pool (8.7×10^5 m^3). Four downstream control points (i.e., New Braunfels NBRT2, Gonzales GNLT2, Cuero CUET2, and Victoria VICT2; National Weather Service, 2018) with the same channel streamflow limit (340 m^3/s) were designated to represent the downstream flow-control operations. The reservoir parameters include the water demand, the discharge rate from the reservoir, and the flood inflow threshold (Zhao et al., 2016b). The monthly water demand data for each reservoir was calculated based on the water rights and water use data, which were derived from the Texas Commission on Environmental Quality (2017). The discharge rate from the reservoir and the flood inflow threshold were calibrated based on a comparison between the simulated and observed reservoir storage.
- Two types of **meteorological forcing data** — observation-based and synthetic —were utilized in this study. Both datasets contain a full set of meteorological forcing terms (i.e., air temperature, wind speed, relative humidity, incoming shortwave radiation, incoming longwave radiation, and precipitation). The observation-based forcing data were obtained from Livneh et al. (2013), which are available for the CONUS at 1/16° spatial resolution and a daily time step from 1915 to 2011. To explore the sole influence of urbanization on flooding, an alternative synthetic forcing dataset—which does not exhibit any precipitation interannual variability (i.e., having the same annual precipitation each year)—was created for the SARB. 1975 was selected as the representative year for the SARB mainly because the annual mean precipitation in 1975 (832 mm) was close to the multi-year annual mean observed precipitation from 1966 to 2011 (813 mm). Additionally, the intra-annual precipitation distribution of 1975 is similar to the SARB precipitation climatology when compared to other years. Moreover, there were neither extremely wet nor extremely dry events in 1975. Next, the cumulative distribution function (CDF) mapping technique was applied. The 1975 daily precipitation was first organized as a look-up table. During each year, the quantile of daily precipitation was determined and then used to identify the corresponding quantile in the 1975 table. Then it was replaced by the value from the look-up table. This led to a synthetic forcing dataset that had identical daily precipitation distribution values for each year. The concept of this approach is similar to that of the Quantile Mapping (QM) method, which is widely used to post-process downscaled GCM projections (Wood et al., 2002; Wood & Lettenmaier, 2006). This method can facilitate the removal of inter-annual variations of the precipitation data while preserving its physical characteristics. Both datasets were then disaggregated to a 3-hourly time step. Further details about the synthetic forcing data can be found in the Supplementary Material.

3.2. Model set up and study design

3.2.1. DHSVM-Res calibration and validation

The calibration and validation processes were conducted for the GRB. The calibrated parameters for the SARB were adopted from Zhao et al. (2016a) (Table S4). The calibration was performed individually for each subbasin of the GRB from January 1, 2001 to December 31, 2011, and the simulation was conducted under NLCD2006 using observation-based forcing data. Ten USGS streamflow gauges (Fig. 1) were selected for the two basins based on their locations and the available data lengths. Calibration based on multiple gauges across the entire river basin can also facilitate the testing of the model's performance and can reduce over-fitting issues.

The calibration of the soil and vegetation parameters was conducted by comparing the simulated streamflow—and the simulated monthly maximum streamflow—with the observed streamflow at four USGS stations (i.e., USGS 08167500, USGS 08171300, USGS 08173900, and USGS 08175800). Based on a sensitivity test (Zhao et al., 2016a), streamflow was found to be most sensitive to six soil/vegetation parameters — lateral hydraulic conductivity, maximum infiltration, soil porosity, wilting point, field capacity, and monthly leaf area index. The reservoir parameters were calibrated afterward by comparing the simulated and observed reservoir storage values. Three criteria were used for the calibration: the Nash Sutcliffe Efficiency (NSE; Nash & Sutcliffe, 1970), the coefficient of determination (R^2), and the relative bias (RB).

The validation was conducted from January 1, 1966 to December 31, 2011 by comparing the simulated streamflow with the observed streamflow at USGS 08175800. The simulation was conducted under LC1970, NLCD1992, NLCD2001, NLCD2006, and NLCD2011 using the observation-based forcing data. The results of the calibration and the validation for the GRB are shown in Section 4.1.

3.2.2. Study design

The impacts of urbanization on flooding were studied comprehensively through a series of comparative analyses between the paired basins (Table 1). Considering that the change in land cover due to urbanization affects floods in many aspects, three sets of analyses were designed. First, to study the influence of urbanization on the change of flood characteristics (i.e., flood peak, peak time), the analysis was performed for two specific flood events by comparing the observed and

Table 1
Summary of the designed analyses.

Purpose	Focus on variables	Basin	Inputs for simulation		Periods for simulation
			Landcover map	Forcing source	
Analyzing flooding events	Q	GRB	LC1970	Observed	Dec 1, 1986 – Jan 31, 1987; Oct 17, 2002 – Dec 1, 2002
		SARB			
Detecting CP of monthly floods	[1]MMS, [2]nMMS	GRB	LC1970	Observed	1968-2006
	MMS	SARB			
	[3]RX5day	GRB			
		SARB			
Testing elasticity of long-term flood regimes	[4]MMS_{50}	SARB	LC1970	Observed	1986-2011
			CLCS ULC1986*	Synthetic	
		GRB	LC1970	Observed	

*The constructed CLCS of 1986, which was created using the baseline map — LC1970 — and the urban land cover maps of 1986.
[1]MMS represents the monthly maximum streamflow time series and was derived from the 3-hourly streamflow.
[2]nMMS represents the monthly maximum streamflow time series without the impacts of reservoir regulation.
[3]RX5day represents the monthly maximum of consecutive 5-day precipitation time series.
[4]MMS_{50} represents the median of the monthly maximum streamflow time series.

simulated daily mean streamflow (Q) for the paired basins. Then, to study the influence of urbanization on the change of monthly floods (e.g., statistical distribution), the distributions of three variables were investigated via change point (CP) analysis and percentile analysis. These three variables are: the observed monthly maximum consecutive 5-day precipitation time series (RX5day), which is an important metric to indicate monthly floods (Karl et al., 1999; Peterson et al., 2001; Wang et al., 2017); the observed/simulated monthly maximum streamflow time series (MMS), representing the monthly peak streamflow series (Zhang et al., 2011); and the observed/simulated monthly maximum naturalized streamflow time series (nMMS), indicating the MMS without the impact from reservoir regulation. Finally, to test the sensitivity of the status of long-term flood regimes to different urban land covers, a newly defined elasticity test was conducted that studied the median of the monthly maximum streamflow time series (MMS_{50}). The above three steps are explained in detail below.

First, the observed daily mean streamflow (Q_{obs}) and the simulated daily mean streamflow using LC1970 (Q_{LC1970}) were analyzed for the paired basins over two periods — December 1, 1986 to January 31, 1987, and October 17, 2002 to December 1, 2002. This analysis is based on the streamflow data from USGS 08175800 and USGS 08188500, which are the main downstream stations of the paired basins, respectively. For each flood event during the two periods, the differences in the peak time and the peak magnitude between Q_{obs} and Q_{LC1970} were compared for the paired basins. The purpose of using the fixed LC1970 for Q_{LC1970} is to eliminate the effects of urbanization to isolate the influence of the changing climate.

Second, the CP detection method (Killick & Eckley, 2014) was utilized to detect the abrupt changes of the long-term underlying distributions of RX5day, MMS, and nMMS. This method was developed based on a maximum likelihood estimation framework and has been applied to a number of hydrological time series in past studies (Harder et al., 2015; Gu et al., 2017; Li et al., 2017; Liu et al., 2017; Sidibe et al., 2018). Before implementing this method, the flood peaks of the historical flood events were analyzed. The October 1998 flood peak was the highest peak on record for both the GRB and the SARB. This flash flood was caused by two hurricanes in the Eastern Pacific (i.e., Hurricane Madeline and Hurricane Lester) and a relatively stationary cold front (White, 2018; National Weather Service, 2019; U.S. Geological Survey, 2014). Thus, this extreme event was considered as an outlier, which greatly impacted the statistics of the dataset (e.g., mean and standard deviation). Thus, the values of RX5day and the flood peaks in October 1998 were removed from all datasets for both basins at the locations of USGS 08175800 and USGS 08188500 (which are the main downstream stations of the paired basins). Then, the CPs of RX5day, the observed MMS (MMS_{obs}), and the simulated MMS under the fixed LC1970 (MMS_{LC1970}) were calculated for both basins. Because there are no major reservoirs in the SARB, the CP of the simulated nMMS under the fixed LC1970 ($nMMS_{LC1970}$) was not tested for the SARB. After the CP detection, percentile analyses were conducted for RX5day, MMS_{LC1970}, and MMS_{obs}.

Third, an elasticity test was conducted for two purposes: (1) comparing the elasticity of precipitation between the paired basins, and (2) assessing the isolated influence of the progressive urbanization process on MMS_{50}. Correspondingly, there were two sets of simulations processed from 1986 to 2011 to facilitate the elasticity tests: (1) the first set was processed under the same fixed land cover map (i.e., LC1970); (2) the second set was conducted using the CLCS and a single fixed land cover (i.e., ULC1986) for the SARB. The elasticity test was originally introduced by Schaake (1990) and was designed for evaluating the sensitivity of the annual mean streamflow to changes in annual precipitation. A similar but modified test was performed in this study based on simulations that were conducted under different urban land cover scenarios and were forced by a series of perturbed precipitation patterns. The elasticity of MMS_{50} is defined as:

$$\varepsilon_p(P', Q') = \frac{dQ'/Q'}{dP'/P'} \quad (1)$$

where Q' represents MMS_{50}, and P' represents the perturbed observed/rescaled precipitation. In the first set of the elasticity tests, the observation-based precipitation (Livneh et al., 2013) was perturbed such that the interannual variations of the historical precipitation data could be preserved. In the second set of the elasticity tests, the rescaled synthetic precipitation was perturbed, which is free of the interannual variations resulting from the use of the CDF mapping technique. In both sets, the precipitation values have been changed by ± 10%, ± 20%, and ± 30%. The test was conducted for the entire SARB, and focuses on the simulated streamflow at USGS 08188500. However, for the GRB, the elasticity test was only conducted for the San Marcos River subbasin (Fig. 1; a subbasin of the GRB), and the simulated streamflow was targeted at USGS 08173900. This is due to the fact that the main soil type of the upper Guadalupe River Basin is clay loam (Fig. S1, Supplementary Material), which is different from the major soil types of the other subbasins of the GRB—and those of the entire SARB. The San Marcos River subbasin is also representative for the GRB in terms of the DEM, land cover, and precipitation distribution. For the DEM, most subbasins are in the region of low elevation—except the upper GRB, and the upper portion of San Marcos River subbasin. Thus, the DEM for San Marcos River subbasin can be representative of the whole GRB. The San Marcos River subbasin contains two major land cover types (grass and forest), while other subbasins are dominated by just one land cover type (forest in the Upper GRB, and grass in the Middle GRB and Lower GRB). Additionally, the monthly precipitation distribution in the San Marcos River subbasin is almost the same as that of the entire GRB.

4. Results

4.1. DHSVM-Res calibration and validation

The calibration and validation results for the GRB are shown in Fig. 3. The error statistics of the daily calibration for the Lower GRB

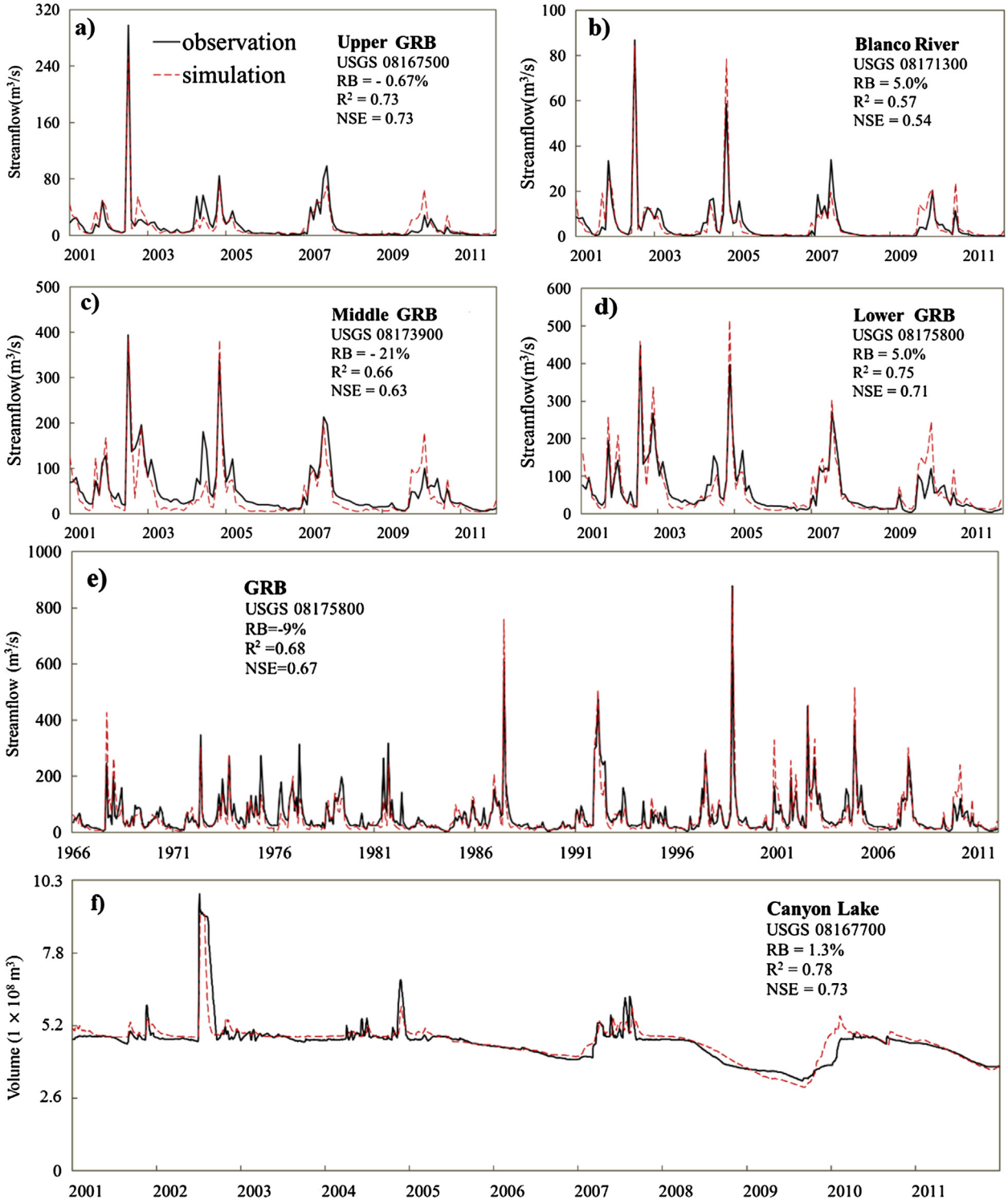

Fig. 3. Results of the calibration (January 2001– December 2011) and the validation (January 1966 – January 2011) in the GRB. a) – d) Calibration of the daily streamflow for each subbasin. e) Validation of the daily streamflow over the entire GRB. f) Calibration of the monthly reservoir volume for the Canyon Lake Reservoir. The statistics in a) – e) are all based on daily results but are shown as monthly average results for showing general hydrograph.

suggest that the simulated streamflow is relatively accurate with an R^2 of 0.75, an NSE of 0.71, and an RB of 0.05 (Fig. 3d). However, the results for the Blanco River gauge station (Fig. 3b) are not as good, with both the R^2 and the NSE under 0.60. Meanwhile, it is observed that the simulated base flows do not agree very well with the observations in some subbasins (Fig. 3b, c, and d), which can be attributed to groundwater discharge from the Edwards Aquifer close to USGS 08171300 near Kyle, Texas. Regardless, the good agreement of the simulated and observed reservoir storage volume for Canyon Lake indicates that the reservoir parameters in DHSVM-Res are robust (Fig. 3f). The error statistics of MMS were also calculated for both basins, and the results show that the simulated MMS are relatively accurate (with R^2 values of 0.84 and 0.78, and NSE values of 0.78 and 0.77 for the GRB and the SARB, respectively). The validation results (Figs. 3f and 4) indicate that the calibrated parameters can simulate the daily streamflow and the MMS for both basins.

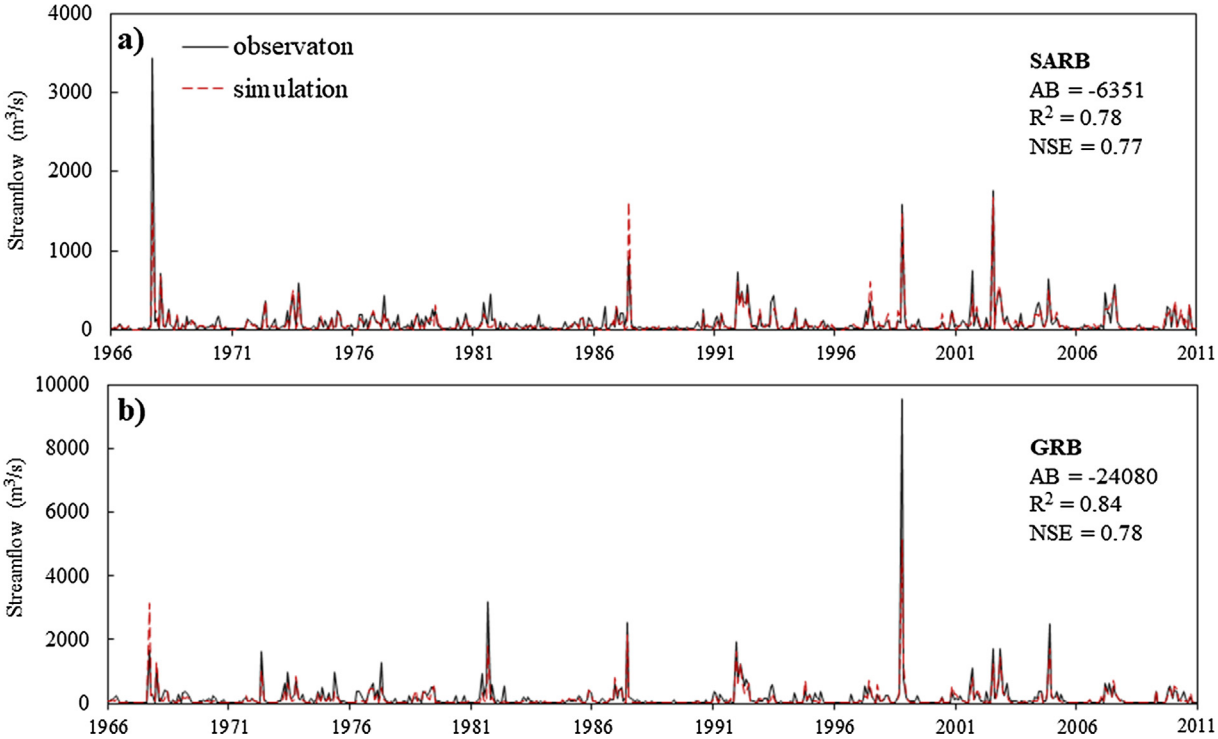

Fig. 4. Validation results for MMS in the GRB and SARB from 1966 to 2011. © American Meteorological Society. Used with permission.

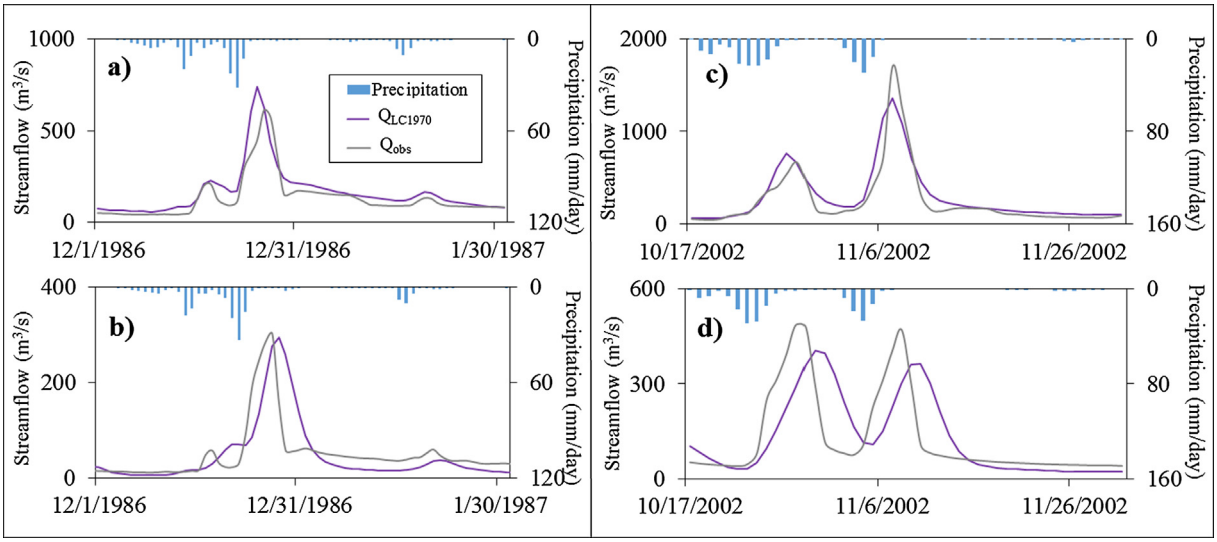

Fig. 5. The observed and the simulated daily mean streamflow for the GRB and the SARB. The purple lines represent Q_{LC1970}, and the grey lines represent Q_{obs}. a) Q_{obs} and Q_{LC1970} from December 1, 1986 to January 31, 1987 for the GRB. b) Q_{obs} and Q_{LC1970} from December 1, 1986 to January 31, 1987 for the SARB. c) Q_{obs} and Q_{LC1970} from October 17, 2002 to December 1, 2002 for the GRB. d) Q_{obs} and Q_{LC1970} from October 17, 2002 to December 1, 2002 for the SARB. (For interpretation of the references to colour in this figure legend, the reader is referred to the web version of this article.)

To evaluate the simulated timing of peak flow events, several flood events with similar magnitude to the flood events in Fig. 5 are selected to calculate the lag time between the observed and simulated peak flow timing. Results shown in Tables S5 and S6 of the Supplementary Material indicate that the model can accurately simulate the peak time on a daily scale in 43% of the selected events in the SARB and in 68% of those in the GRB.

4.2. Comparisons between SARB and GRB

4.2.1. Comparisons of streamflow during flood events

To evaluate the impacts of urbanization on flood events, the flood peak and peak time were compared between Q_{obs} and Q_{LC1970} for the paired basins over two selected periods (i.e., December 1, 1986 to January 31, 1987; October 17, 2002 to December 1, 2002) —a time period during which the two basins had similar precipitation events and similar hydrological responses (Fig. 5).

First, Q_{obs} and Q_{LC1970} were compared from December 1, 1986 to January 31, 1987. For the GRB, the peak of Q_{obs} was 612 m^3/s on December 26, 1986, which was 17% smaller than that of Q_{LC1970} on December 25, 1986 (739 m^3/s; Fig. 5a). This might be attributed to model uncertainties. For the SARB (Fig. 5b), the peak of Q_{obs} was 303 m^3/s on December 27, 1986, which was slightly higher and 1 day earlier than Q_{LC1970} (295 m^3/s peaked on December 28, 1986). The

impervious area increased from 3.0% in 1970 to 4.9% in 1986 estimated from the CLCS, which could lead to an acceleration of runoff process resulting in the observed elevation of the flood peak.

Then, Q_{obs} and Q_{LC1970} in the GRB and the SARB were compared from October 17, 2002 to December 1, 2002 (a period which contains two flood events). For the GRB, the first peak of Q_{obs} was 668 m^3/s on October 28, 2002, which was slightly lower than that of Q_{LC1970} (761 m^3/s) on October 27, 2002 (Fig. 5c). The second peaks of Q_{obs} and Q_{LC1970} were 1705 m^3/s and 1361 m^3/s respectively, which both occurred on November 7, 2002 (Fig. 5c). This can be possibly attributed to model uncertainties and uncertainties associated with the land cover data. First, the classification algorithms are different for LC1970 and other NLCD products, which may add uncertainties to the simulated streamflow. Second, based on the data shown in Table S7 (Supplementary Materials), the impervious area increased 0.19% from LC1970 to NLCD2001—with a slight decrease in bare ground, grassland, and forest. The higher second peak flow in the Q_{obs} compared with Q_{LC1970} could be also related to these land cover changes, which were not addressed in the model scenarios. For the SARB, the first peak of Q_{obs} was 484 m^3/s on October 28, 2002. This is about 20% larger than that of Q_{LC1970} (406 m^3/s), which occurred on October 30, 2002 (Fig. 5d). The second peak of Q_{obs} was 470 m^3/s on November 8, 2002, which is 30% larger than that of the corresponding Q_{LC1970} (363 m^3/s) on November 10, 2002 (Fig. 5d). The comparison between Fig. 5c and Fig. 5d suggests that urbanization exacerbated the effects of antecedent moisture conditions on floods. In the SARB, the difference between the second peaks (30%) is noticeably larger than that of the first flood peaks (20%). When comparing Fig. 5b and d, the difference between the lag times is two days for both flood events in 2002 and only one day for the flood events in 1986. These differences might be attributed to the increase in impervious area (i.e., 6.5%), the higher catchment's antecedent moisture content, and/or the larger flood size in 2002 (as compared to 1986). It can be inferred that urbanization effects outweigh the model uncertainty and are apparent in the SARB.

4.2.2. Change point analysis

The results of the detected CPs are summarized in Table 2. The CPs of RX5day were detected in terms of variance, and the CPs of other variables (i.e., MMS_{obs}, MMS_{LC1970}, and $nMMS_{LC1970}$) were detected in terms of mean. All CPs were detected at a significance level of 5%. The CPs of RX5day were not detected in terms of mean because the variation of mean value of RX5day was relatively small, and the CP of the mean value of RX5day was undetectable at a significance level of 5%. When comparing the mean/variance of the post-CP period with the pre-CP period for the above four variables, the mean/variance of the post-CP period was larger than that of the pre-CP period in all cases (Table 3).

The CPs of RX5day were first compared for the paired basins to assess if the two basins had undergone similar climate patterns. The CP of RX5day for the GRB was in October 1991, which was close to the CP of RX5day for the SARB (i.e., April 1990). This indicates that the RX5day of the two basins share similar change patterns, which makes them suitable for *paired catchments* analysis. Next, the CPs of MMS_{obs} and MMS_{LC1970} were detected for these basins. For the GRB, the CPs were also in October 1991 (for both MMS_{obs} and MMS_{LC1970}), which is in agreement with the CP of RX5day. The results show that the change of flood pattern mainly depends on the changing climate when there is limited or no LUCC.

Table 3
Differences (%) between the post-CP and the pre-CP periods.

Basin	Variable	RX5day	MMS_{obs}	MMS_{LC1970}	$nMMS_{LC1970}$
GRB	mean	6.5%	24.7%	46.1%	44.5%
	variance	39.1%	25.8%	69.0%	58.3%
SARB	mean	5.4%	75.7%	37.9%	
	variance	57.9%	440.0%	65.5%	

For the SARB, the CP of MMS_{LC1970} was also October 1991 — the same for the GRB. However, the CP of MMS_{obs} was June 2001, with its mean value increased by 75.7% from the pre-CP period to the post-CP period (Table 3). In contrast, the mean value of MMS_{obs} only grew by 24.7% for the GRB, even though the RX5day of the GRB had a larger gain (6.5%) than that of the SARB (5.4%). The significant change of MMS_{obs} for the SARB after June 2001 could be linked to the high-speed urbanization of San Antonio — with the impervious area increasing at an average annual rate of around 3% from 2001 to 2007, and the population growing at an average annual rate of 15.9% from 2000 to 2010 (Castro et al., 2012). This continuous urbanization amplified the effects of the changing climate (i.e., the change of RX5day) on streamflow, and thus elevated the value of MMS significantly (and even changed the timing of the CP of MMS).

For the GRB, the CPs of $nMMS_{LC1970}$ and MMS_{LC1970} were both in October 1991—with the average of $nMMS_{LC1970}$ being 10% larger than that of MMS_{LC1970}. This suggests that the construction of the reservoir has changed the natural hydrological process by lowering the MMS. Additionally, the same change points of the variables (October 1991; Table 2), and the similar differences of $nMMS_{LC1970}$ and MMS_{LC1970} (Table 3), show that the monthly floods also vary significantly according to the change of RX5day.

Next, the mean value of each of the following—RX5day, MMS_{obs}, and MMS_{LC1970}, within each 10th percentile—was calculated in both the pre-CP and post-CP periods (CP: October 1991). The difference between the mean values of the pre-CP and post-CP periods was then calculated for each of the ten percentile ranges. Fig. 6 shows the partitioning of the total difference according to the variable's percentile range. Because the difference values are very small in the 1–70 percentile range, these are summed together. As shown in Fig. 6, the major differences of the three variables (i.e., RX5day, MMS_{obs}, and MMS_{LC1970}) are all found within the 90th to 100th percentile. This suggests that the changes detected are primarily associated with extreme rainfall or extreme peak flows. For the GRB, the difference value for each percentile range is very similar among the three variables. For the SARB, the difference of the MMS_{obs} in the 90th – 100th percentile range is clearly larger than those of the RX5day and MMS_{LC1970}—indicating that the urbanization in the SARB after 1991 has exacerbated the impact of changing precipitation on the peak flows.

4.2.3. Elasticity tests

There were two sets of elasticity tests conducted from 1986 to 2011 (Fig. 7). In general, elasticity increases when there is more precipitation because larger precipitation can lead to more surface runoff and therefore is more likely to cause a larger rainfall-runoff ratio. However, the differences among the elasticities of the two urban conditions are relatively small when compared with those of the variously disturbed

Table 2
Summary of the change point analysis.

Basin	GRB				SARB		
Variable	RX5day	MMS_{obs}	$nMMS_{LC1970}$	MMS_{LC1970}	RX5day	MMS_{obs}	MMS_{LC1970}
CP (month/year)	10/1991	10/1991	10/1991	10/1991	04/1990	06/2001	10/1991

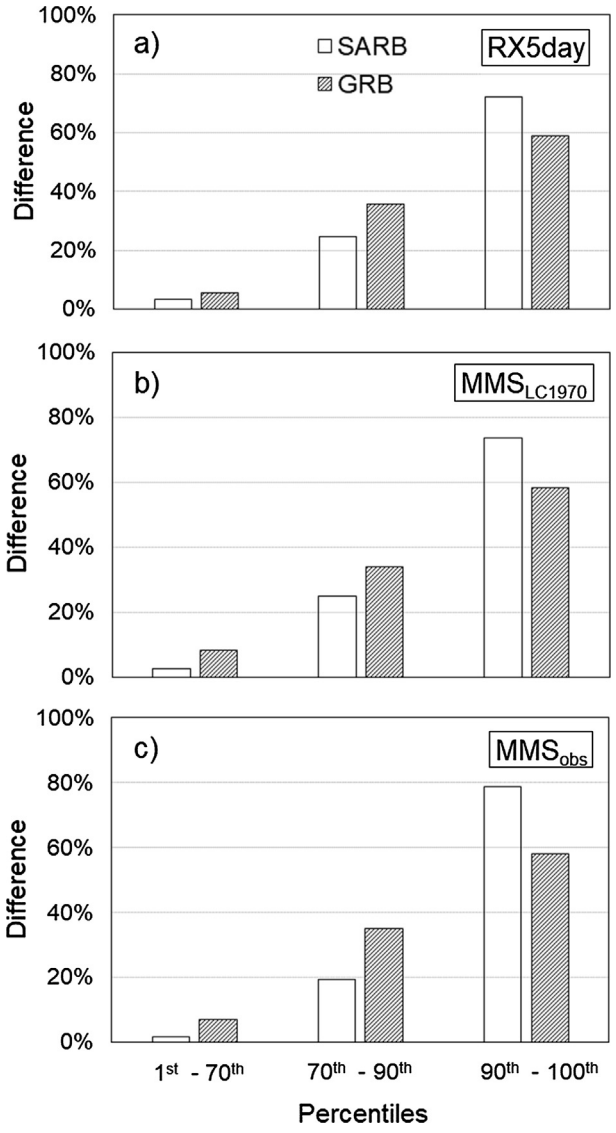

Fig. 6. The differences in RX5day, MMS_{obs}, and MMS_{LC1970} before and after Oct 1991 at different percentiles for the SARB and the GRB. a) The differences in RX5day. b) The differences in MMS_{LC1970}. c) The differences in MMS_{obs}.

precipitation series.

The comparison of the elasticities between the paired basins is shown in Fig. 7a. The simulations were processed for the paired basins under the same fixed land cover map (i.e., LC1970) and the same observation-based forcing data. Considering that there was a relatively small amount of urbanized land in the paired basins in the 1970s, elasticity mainly depended on basin characteristics and forcing data. The elasticity ranges from 1.71 to 2.82 for the GRB, which is similar to that of the SARB (1.69 to 2.76). The elasticities of the GRB are slightly larger than those of the SARB in the case of 30% precipitation. In the cases of 10% and 20% precipitation, however, the elasticities of the SARB are slightly larger than those of the GRB. Nevertheless, it is evident that the elasticity values of the paired basins resemble each other. This analysis also supports using the *paired catchments* comparison approach for this study.

The evaluation results showing the isolated impacts of the progressive urbanization process on MMS_{50} are shown in Fig. 7b. The elasticity was tested under two types of land cover maps and was synthetically forced over the SARB. One land cover map is CLCS, and the other is the fixed CLCS with 1986 urban land cover (i.e., ULC1986). In the case of ULC1986, the elasticity ranges from 1.77 to 2.81. In the case of CLCS, the elasticity ranges from 1.74 to 3.02 (Fig. 7b). The elasticity of CLCS is obviously larger than that of ULC1986 in most perturbed precipitation scenarios, except in the case of −30% precipitation (where the elasticity of ULC1986 is slightly larger than that of CLCS). This can be attributed to two reasons: First, when the precipitation is relatively small, most of it becomes evapotranspiration and soil moisture (where little can reach the basin outlet in the form of overland flow or base flow). Second, when there is more impervious area, DHSVM-Res is set up such that a higher portion of the surface runoff goes into the urban channel. This is due to the low infiltration capacity of impervious surface, and the quick routing process — so less surface runoff is available to infiltrate into the deep soil, and less is available to evaporate on the land surface. Despite this, continuous urbanization still plays a primary role in elevating the elasticity of MMS_{50}.

5. Discussion

The *paired catchments* approach has a unique advantage because it uses observed precipitation and streamflow data to complement the modeling approaches and quantify the urbanization impact. For instance, the change point analysis that we performed (Section 4.2.2) has shown that by comparing the statistics of observed precipitation and streamflow over the paired basins, the effects of urbanization within the

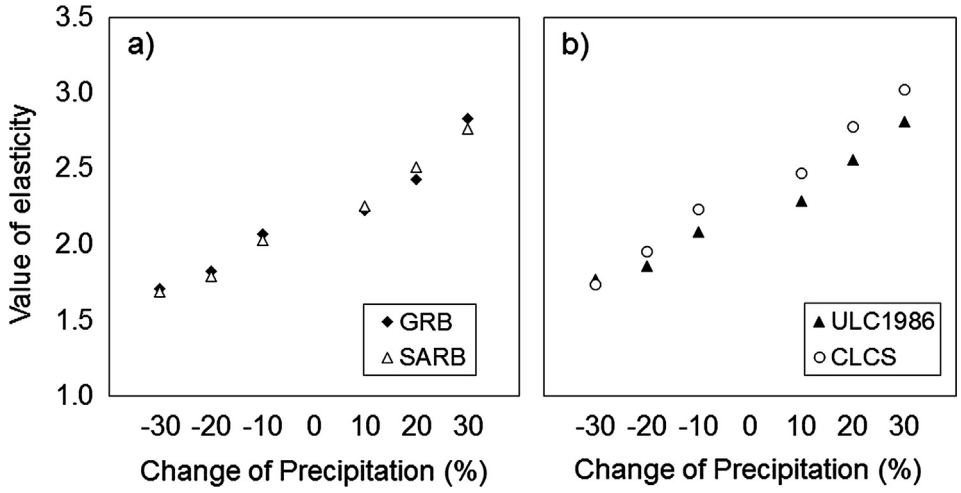

Fig. 7. The results of the elasticity test under different scenarios. a) The elasticities under LC1970 for the GRB and the SARB. b) The elasticities under the ULC1986 and the CLCS for the SARB.

SARB are isolated. If we only investigate the changes of observed precipitation and streamflow from one basin, it is challenging to separate the urbanization and climate change impacts as their impacts are both included in the observation data. Even though using detrended climate data to drive a model is a well-recognized method, the results can be subject to uncertainties due to the selected period. Therefore, our study uses a hybrid approach that leverages both the *paired catchments* and modeling methods.

It is important to investigate the effects of the changing climate before evaluating the isolated influences of urbanization. In the paired basins, we found that RX5day increased significantly after the 1990s, which is in line with the findings of Kunkel et al. (2010)—who observed that the number of heavy precipitation events associated with tropical cyclones over the CONUS during 1994 to 2008 was more than twice the long-term average.

While many studies show that the changing climate is one main factor affecting streamflow variability, other factors such as urbanization are also closely associated with increasing flood events (Yang et al., 2013; Buendia et al., 2016; Zhao et al., 2016a). We reached a similar conclusion by combining *paired catchments* analysis with a physics-based modeling framework (DHSVM-Res). Furthermore, we disentangled the impacts of urbanization and changing climate on floods using a hydrological model. The application of the fixed LC1970 to the model simulations of the paired basins not only extracted the influences of the changing climate, but also facilitated the evaluation of isolated urbanization effects by comparing Q_{obs} with Q_{LC1970}, and MMS_{obs} with MMS_{LC1970}. The idea of conducting a comparative analysis with fixed land use maps has been previously investigated. For example, the effects of land use change on the flood frequency regime in the Samoggia river basin of Italy were assessed by applying fixed land use scenarios from 1955, 1980 and 1992 (Brath et al., 2006). In this study, nMMS was simulated to eliminate the influences from reservoir regulation on the GRB, which contributes to the rationality of using the GRB as the "reference basin". The elimination of similar "non-target effects" within the "reference basin" is important for other studies (this can be accomplished by various hydrological modeling techniques).

In this study, all subbasins within these two basins were calibrated independently to avoid an overfitting problem which occurs when only the streamflow of the downstream stations was calibrated. While this has improved the overall model performance, it could also add uncertainties to the *paired catchments* approach. Since the validation was conducted over a long time period (46 years from 1966 to 2011), the robust results suggest that the uncertainties associated with this calibration approach are relatively small. As a result, the paired basins do not exactly share the same model parameterization. Furthermore, the calibration was conducted in this way because the model and model parameters are not completely physics-based. Model structure, and model parameters — as well as the forcing and input data (e.g., soil texture) — all have associated uncertainties. Calibration over each subbasin could practically reduce the impacts of these types of uncertainties. Nevertheless, the selection of parameters over the paired basins has not been fully investigated in this study. Thus, more future studies are expected to be conducted using the recently published parallel DHSVM (Perkins et al., 2019) –which is significantly more computational efficient – for evaluating the effects of parameter selection over the neighboring basins.

The elasticity results were also compared against a contour map of precipitation elasticity of streamflow covering the United States, which was developed by Sankarasubramanian et al. (2001) and was widely used as a validation metric in later studies. The map showed that the elasticity values ranged from 0.5 to 3.5 over the United States, and higher values (greater than 2.0) primarily occurred in arid and semiarid regions such as the Southwest and Midwest. In Texas, elasticity values mainly fall into the range of 1.0 – 2.5. Considering that model genres and model calibration also play important roles in determining elasticity values (Sankarasubramanian et al., 2001; Dooge, 1992), the elasticity results of this study are reasonable and can be compared with those of future research.

The application of synthetic forcing data in elasticity tests significantly eliminated the influences of the changing climate, which made the isolated evaluation of urbanization influences even more thorough. The CDF mapping technique borrows this idea from the QM method, which is widely used to post-process downscaled GCM projections (Wood et al., 2002; Wood & Lettenmaier, 2006). When creating synthetic forcing data, the selection of a representative year is an important step. Here we mainly consider the similarity of annual mean precipitation and intra-annual precipitation distribution between the selected year and the climatology. However, there are still uncertainties inherent to this method. Experiments using different representative precipitation years are expected to be conducted in the future. Nevertheless, this CDF mapping technique creates the rescaled precipitation of the synthetic forcing data (Text S2 in Supplementary Material) — which is a simple and transferrable method.

In most hydrological modeling studies over the United States, four NLCD land cover maps (i.e., NLCD1992, NLCD2001, NLCD2006, and NLCD2011) have been applied to simulate the change in land cover. However, the unavailability of continuous land cover maps hinders the continuous quantification of the effects of LUCC on hydrologic processes (Fletcher et al., 2013; Zarezadeh & Giacomoni, 2017). This is because LUCC influences the energy balance and the hydrological cycle (Zhu & Woodcock, 2014). In this sense, using annually continuous LUCC maps to parameterize the model is the ideal choice for realistic evapotranspiration and surface runoff results. However, our newly developed CLCS only provided continuous LUCC changes for urban areas and did not include changes for non-urban land use types. This is primarily because our focus is on urbanization, which has the most significant impacts on altering surface runoff as compared to other land cover changes. Meanwhile, other non-urban land cover types did not change as much as urban land cover in the SARB. To our knowledge, a product named LCMAP (Land Change Monitoring, Assessment, and Projection), which includes annual LUCC maps (from 1985 to 2017) in the United States, is under development (U.S. Geological Survey, 2020). This product can be used in future studies to facilitate sustainable land management and to better evaluate the hydrological responses to LUCC. In addition, a free and advanced cloud-computing geospatial platform—the Google Earth Engine (GEE; Gorelick et al., 2017)—was used to develop the CLCS used in this study. The analysis scripts and results have been released on GEE (https://code.earthengine.google.com/a71de59b8522e79ba401ccb4f63f1d55), which makes the classification methods transferrable to many other urbanized basins throughout the world.

With regard to CP detection, historical analyses have mainly been based on either total or mean streamflow over multiple years (Gao et al., 2010; Harrigan et al., 2014; Cockburn & Garver, 2015; Buendia et al., 2016; Ivancic & Shaw, 2017). Also, a limited number of CP analyses have been performed on flood-related variables at a monthly level. Our work expands the use of CP to support further exploration of anthropogenic influences on floods.

Even though our work can deliver useful information for local water resources management, some limitations need to be addressed in future studies:

1) Only satellite images collected by the Landsat 5 TM sensor from 1984 to 2011 were used. The length of the study period can be extended to more recent years by incorporating images collected by Landsats 7 and 8, which will be more informative to current and near-future water resources management practices.
2) Table S7 of the Supplementary Material shows a slight increase in forested area from LC1970 to NLCD1992. However, there could be uncertainties associated with the LC1970 land cover data because the classification methodology is different for LC1970 when compared with that of other NLCD products (Price et al., 2006).

Research is necessary to obtain more accurate historical land cover maps, which have consistent classification with the current NLCD products.

3) The calibration and validation results (Fig. 3) suggest that the capabilities of DHSVM-Res in base flow simulations are limited, which hinders further applications of DHSVM-Res. In the future, this limitation can be alleviated by coupling a complete groundwater component to the current modeling framework.
4) The impacts of urbanization on regional climate were not considered. Other modeling systems such as the Weather Research and Forecasting (WRF) model can be used in the future to capture the influences of urbanization on regional climate.
5) The elasticity test uses MMS_{50}, which is different from the traditional estimator (i.e., the average streamflow). The reason is that limited research campaigns have investigated MMS_{50}, so this study could provide quantitative information regarding the sensitivity of the long-term monthly flood regime to precipitation. Furthermore, only one normal year (1975) was selected as the representative year, and thus the uncertainties regarding the selection of the representative years have not been fully investigated. More precipitation scenarios—using wet or dry years as the representative year—should be included in future elasticity studies. Additionally, the simulations for the elasticity test can be extended by including a future climate sensitivity test, via the application of regional climate models (Feser et al., 2011).

6. Conclusion

A large portion of the world's population is facing flood-related risks because of urbanization (Miao, 2018), and it is imperative to study the impacts of urbanization on flooding. Considering the widescale accessibility of various remote sensing datasets, distributed hydrological modeling can be conducted in many other paired river basins. Hence, our comparative investigation, based on *paired catchments* analysis and a modeling framework, is transferrable to other regions of the world to promote local water security. Overall, this study evaluates the influence of urbanization on flooding and unravels the combined impacts of urbanization and the changing climate to improve water security. Our main findings include:

1) The GRB and SARB are reasonably paired basins for studying the effects of urbanization on floods. They share similar physical characteristics and analogous elasticities of precipitation. Additionally, the urban impervious area of the SARB has increased significantly, while the land cover of the GRB has scarcely changed.
2) With paired basins and a comprehensive modeling framework, this study separated the impacts of the changing climate and urbanization and removed the effects of reservoir regulation. Thus, the influence of urbanization on flooding was extracted.
3) The change of MMS patterns was mainly driven by the changing climate when there was limited LUCC. The evidence is the same CP – October 1991 – among the RX5day, MMS_{obs} and MMS_{LC1970} for the GRB, as well as MMS_{LC1970} of the SARB.
4) Through analysis of the selected flood events, we found that urbanization can cause an apparent elevation of flood peaks, lead to shorter lag times, and exacerbate the influence of antecedent moisture conditions on floods. During the flood events over the SARB in 2002, the flood peak of Q_{obs} was two days earlier than that of Q_{LC1970}—and the difference between the peaks of Q_{LC1970} and Q_{obs} reached 30%.
5) By detecting the change points (CP) of monthly floods, we found that the high-speed urbanization of San Antonio amplified the effects of the changing climate on streamflow patterns. This elevated MMS significantly, and thus changed the timing of the CP of MMS_{obs} to June 2001. Meanwhile, the difference between the values of the post-CP and the pre-CP periods of MMS_{obs} for the SARB was around 76%, which was obviously larger than that for any of the other cases.
6) The elasticity test confirmed that continuous urbanization played a primary role in elevating the elasticity of MMS_{50} when the influence of the changing climate was eliminated to a significant level. The differences among the elasticities of the two urban land cover scenarios became larger with increased precipitation.
7) While flow regulation reduced the peak flow values and lessened the streamflow intra-annual variability, it did not affect the CP. For instance, in the GRB we found that the variance is larger for MMS_{1970} (69%) than for $nMMS_{1970}$ (58.3%; Table 3)—but the CPs of MMS_{LC1970} and $nMMS_{LC1970}$ were the same as that of RX5day – October 1991.

This study successfully quantified the impacts of urbanization on floods in a systematic manner by using *paired catchments* analysis and DHSVM-Res in two adjacent basins. More studies about the changes of hydrological processes under a changing environment (e.g., urbanization, climate change) are needed in the future.

Credit authorship contribution statement

Manqing Shao: Conceptualization, Methodology, Formal analysis, Investigation, Writing - original draft, Visualization. **Gang Zhao:** Methodology, Software, Resources, Data curation. **Shih-Chieh Kao:** Conceptualization, Resources, Writing - review & editing, Funding acquisition. **Lan Cuo:** Conceptualization, Resources, Writing - review & editing. **Cheryl Rankin:** Resources, Writing - review & editing. **Huilin Gao:** Conceptualization, Writing - review & editing, Supervision, Project administration, Funding acquisition.

Declaration of Competing Interest

The authors declare that they have no known competing financial interests or personal relationships that could have appeared to influence the work reported in this paper.

Acknowledgments

This research was supported by the U.S. National Science Foundation (Grants CBET-1454297 and CBET-1805584), and the U.S. Department of Energy (DOE) Water Power Technologies Office as a part of the SECURE Water Act Section 9505 Assessment. The work has also benefitted from the usage of the Texas A&M Supercomputing Facility (http://hprc.tamu.edu). We appreciate the valuable time that the anonymous reviewers took to review our manuscript and provide the many great suggestions.

Appendix A. Supplementary data

Supplementary data to this article can be found online at https://doi.org/10.1016/j.jhydrol.2020.125154.

References

Alexander, L.V., Zhang, X., Peterson, T.C., Caesar, J., Gleason, B., et al., 2006. Global observed changes in daily climate extremes of temperature and precipitation. J. Geophys. Res. Atmos. 111 (D5). https://doi.org/10.1029/2005JD006290.

Bates, C.G., Henry, A.J., 1928. Second phase of streamflow experiment at wagon wheel gap cold. Monthly Weather Rev. 56 (3), 79–81.

Bosch, J.M., Hewlett, J.D., 1982. A review of catchment experiments to determine the effect of vegetation changes on water yield and evapotranspiration. J. Hydrol. 55, 3–23.

Brath, A., Montanari, A., Moretti, G., 2006. Assessing the effect on flood frequency of land use change via hydrological simulation (with uncertainty). J.Hydrol. 324 (1–4), 141–153. https://doi.org/10.1016/j.jhydrol.2005.10.001.

Brirhet, H., Benaabidate, L., 2016. Comparison of two hydrological models (Lumped and Distributed) over a pilot area of the Issen Watershed in the Souss Basin, Morocco. Eur.

Sci. J. 12 (18). https://doi.org/10.19044/esj.2016.v12n18p347.
Brown, A.E., Zhang, L., McMahon, T.A., Western, A.W., Vertessy, R.A., 2005. A Review of Paired Catchment Studies for Determining Changes in Water Yield Resulting from Alterations in Vegetation. J.Hydrol. 310 (1–4), 28–61. https://doi.org/10.1016/j.jhydrol.2004.12.010.
Buendia, C., Batalla, R.J., Sabater, S., Palau, A., Marcé, R., 2016. Runoff trends driven by climate and afforestation in a Pyrenean Basin. Land Degrad. Dev. 27 (3), 823–838. https://doi.org/10.1002/ldr.2384.
Burns, D., Vitvar, T., McDonnell, J., Hassett, J., Duncan, J., et al., 2005. Effects of suburban development on runoff generation in the Croton River Basin, New York, USA. J. Hydrol. 311 (1–4), 266–281. https://doi.org/10.1016/j.jhydrol.2005.01.022.
Castro, J., Bernal, D.M., Taylor, I. R., Ozuna, L., Saldaña, R.A., et al., 2012. Demographic Distribution and Change 2000 to 2010 Summary Report. Accessed in March, 2018 from https://www.census.gov/prod/cen2010/briefs/c2010br-01.pdf.
Cockburn, J.M.H., Garver, J.I., 2015. Abrupt Change in Runoff on the North Slope of the Catskill Mountains, Ny, USA: above average discharge in the last two decades. J. Hydrol.: Reg. Stud. 3, 199–210. https://doi.org/10.1016/j.ejrh.2014.11.006.
Cross, R., Granato, J., Pinto, P., Jones, M., & Stein, R., 2018. Hurricane Harvey: Experiences, Consequences and Public Support for Proposed Policies. in: Paper presented at the Urban Flooding & Infrastructure Conference: Moving forward from Harvey, Rice University (Accessed in May, 2019).
Cuo, L., 2016. Land use/cover change impacts on hydrology in large river Basins. Terrest. Water Cycle Clim. Change 103–134. https://doi.org/10.1002/9781118971772.ch6.
Cuo, L., Lettenmaier, D.P., Mattheussen, B.V., Storck, P., Wiley, M., 2008. Hydrologic prediction for urban watersheds with the distributed hydrology–soil–vegetation model. Hydrol. Process. 22 (21), 4205–4213. https://doi.org/10.1002/hyp.7023.
DeFries, R., Eshleman, K.N., 2004. Land-use change and hydrologic processes: a major focus for the future. Hydrol. Process. 18 (11), 2183–2186. https://doi.org/10.1002/hyp.5584.
Döll, P., Fiedler, K., Zhang, J., 2009. Global-scale analysis of river flow alterations due to water withdrawals and reservoirs. Hydrol. Earth Syst. Sci. 13, 2413–2432.
Donat, M.G., Alexander, L.V., Yang, H., Durre, I., Vose, R., et al., 2013. Updated analyses of temperature and precipitation extreme indices since the beginning of the twentieth century: the Hadex2 dataset. J. Geophys. Res.: Atmos. 118 (5), 2098–2118. https://doi.org/10.1002/jgrd.50150.
Donat, M.G., Lowry, A.L., Alexander, L.V., O'Gorman, P.A., Maher, N., 2016. More extreme precipitation in the World's dry and wet regions. Nat. Clim. Change 6, 508. https://doi.org/10.1038/nclimate2941.
Dooge, J.C.I., 1992. Sensitivity of runoff to climate change: a Hortonian approach. Bull. Am. Meteorol. Soc. 73 (12), 2013–2024.
Duan, Z. CreateStreamNetwork, 2018. Github Repository, python version. https://github.com/pnnl/DHSVM-PNNL/tree/master/CreateStreamNetwork_PythonV. (Accessed in January, 2018).
Emmett, E., Costello, S., Lindner, J., Read, B., & Cotter, J., 2018. Urban Flooding & Infrastructure Conference: Moving Forward from Harvey. in: Paper presented at the SSPEED, Rice University, Houston, Texas. Accessed in June, 2019.
Feser, F., Rockel, B., von Storch, H., Winterfeldt, J., Zahn, M., 2011. Regional climate models add value to global model data: a review and selected examples. Bull. Am. Meteorol. Soc. 92 (9), 1181–1192. https://doi.org/10.1175/2011BAMS3061.1.
Fletcher, T.D., Andrieu, H., Hamel, P., 2013. Understanding, management and modelling of urban hydrology and its consequences for receiving waters: a state of the art. Adv. Water Resour. 51, 261–279. https://doi.org/10.1016/j.advwatres.2012.09.001.
Fry, J.A., Xian, G., Jin, S., Dewitz, J.A., Homer, C.G., et al., 2011. Completion of the 2006 National land cover database for the conterminous United States. Photogramm. Eng. Remote Sens. 77 (9), 858–864.
Gain, A.K., Giupponi, C., Wada, Y., 2016. Measuring global water security towards sustainable development goals. Environ. Res. Lett. 11 (12), 124015. https://doi.org/10.1088/1748-9326/11/12/124015.
Gao, P., Zhang, X., Mu, X., Wang, F., Li, R., et al., 2010. Trend and change-point analyses of streamflow and sediment discharge in the Yellow River During 1950–2005. Hydrol. Sci. J. 55 (2), 275–285. https://doi.org/10.1080/02626660903546191.
Giertz, S., Diekkrüger, B., Steup, G., 2006. Physically-based modelling of hydrological processes in a tropical headwater catchment (West Africa) &Ndash; process representation and multi-criteria validation. Hydrol. Earth Syst. Sci. 10 (6), 829–847. https://doi.org/10.5194/hess-10-829-2006.
Gorelick, N., Hancher, M., Dixon, M., Ilyushchenko, S., Thau, D., et al., 2017. Google earth engine: planetary-scale geospatial analysis for everyone. Remote Sens. Environ. 202, 18–27. https://doi.org/10.1016/j.rse.2017.06.031.
Goswami, B.N., Venugopal, V., Sengupta, D., Madhusoodanan, M.S., Xavier, P.K., 2006. Increasing trend of extreme rain events over India in a warming environment. Science 314 (5804), 1442. https://doi.org/10.1126/science.1132027.
Groisman, P.Y., Knight, R.W., Easterling, D.R., Karl, T.R., Hegerl, G.C., et al., 2005. Trends in intense precipitation in the climate record. J. Clim. 18 (9), 1326–1350. https://doi.org/10.1175/JCLI3339.1.
Gu, X., Zhang, Q., Singh, V.P., Shi, P., 2017. Changes in magnitude and frequency of heavy precipitation across China and its potential links to summer temperature. J. Hydrol. 547, 718–731. https://doi.org/10.1016/j.jhydrol.2017.02.041.
Guannel, G., Guerry, A., Faries, J., Thompson, M., Silver, J., et al., 2010. Changes in the Delivery of Ecosystem Services in Galveston Bay, TX, under a Sea-Level Rise Scenario. The Nature Conservancy. (Accessed in March, 2018).
Hall, J., Borgomeo, E., 2013. Risk-based principles for defining and managing water security. Philos. Trans.. Series A, Math., Phys., Eng. Sci. 371 (2002). https://doi.org/10.1098/rsta.2012.0407.
Harder, P., Pomeroy, J.W., Westbrook, C.J., 2015. Hydrological resilience of a Canadian Rockies headwaters basin subject to changing climate, extreme weather, and forest management. Hydrol. Process. 29 (18), 3905–3924. https://doi.org/10.1002/hyp.10596.
Harrigan, S., Murphy, C., Hall, J., Wilby, R.L., Sweeney, J., 2014. Attribution of detected changes in streamflow using multiple working hypotheses. Hydrol. Earth Syst. Sci. 18 (5), 1935–1952. https://doi.org/10.5194/hess-18-1935-2014.
Hejazi Mohamad, I., Markus, M., 2009. Impacts of urbanization and climate variability on floods in Northeastern Illinois. J. Hydrol. Eng. 14 (6), 606–616. https://doi.org/10.1061/(ASCE)HE.1943-5584.0000020.
Hengade, N., Eldho, T.I., 2019. Relative impact of recent climate and land cover changes in the Godavari river basin, India. J. Earth Syst. Sci. 128, 94. https://doi.org/10.1007/s12040-019-1135-4.
Homer, C., Dewitz, J., Fry, J., Coan, M., Hossain, N., et al., 2007. Completion of the 2001 national land cover database for the Conterminous United States. Photogramm. Eng. Remote Sens. 73, 337–341.
Ide, J.i., Finér, L., Laurén, A., Piirainen, S., Launiainen, S., 2013. Effects of clear-cutting on annual and seasonal runoff from a boreal forest catchment in Eastern Finland. For. Ecol. Manage. 304, 482–491. https://doi.org/10.1016/j.foreco.2013.05.051.
Im, S., Kim, H., Kim, C., Jang, C., 2008. Assessing the impacts of land use changes on watershed hydrology using mike she. Environ. Geol. 57 (1), 231–239. https://doi.org/10.1007/s00254-008-1303-3.
Ivancic, T.J., Shaw, S.B., 2017. Identifying Spatial Clustering in Change Points of Streamflow across the Contiguous U.S. Between 1945 and 2009. Geophys. Res. Lett. https://doi.org/10.1002/2016gl072444.
[dataset] Jarvis, A., Reuter, H. I., Nelson, A., & Guevara, E., 2008. Hole-filled SRTM for the globe Version 4, available from the CGIAR-CSI SRTM 90m Database. Retrieved from http://srtm.csi.cgiar.org.
Jha, A.K., Bloch, R., & Lamond, J., 2012. Cities and Flooding a Guide to Integrated Urban Flood Risk Management for the 21st Century. 2012 International Bank for Reconstruction and Development.
Jin, S., Yang, L., Danielson, P., Homer, C., Fry, J., 2013. A comprehensive change detection method for updating the national land cover database to circa 2011. Remote Sens. Environ. 132, 159–175. https://doi.org/10.1016/j.rse.2013.01.012.
Jongman, B., 2018. Effective adaptation to rising flood risk. Nat. Commun. 9 (1), 1986. https://doi.org/10.1038/s41467-018-04396-1.
Karl, T.R., Nicholls, N., & Ghazi, A., 1999. CLIVAR/GCOS/WMO Workshop on Indices and Indicators for Climate Extremes Workshop Summary. in: Karl, T.R., Nicholls, N., Ghazi, A. (eds.). Weather and Climate Extremes. Springer, Dordrecht.
Kaushal, S.S., Groffman, P.M., Band, L.E., Shields, C.A., Morgan, R.P., et al., 2008. Interaction between urbanization and climate variability amplifies watershed nitrate export in Maryland. Environ. Sci. Technol. 42 (16), 5872–5878. https://doi.org/10.1021/es800264f.
Killick, R., Eckley, I.A., 2014. Changepoint: an R package for changepoint analysis. J. Stat. Softw. 58 (3).
Kottek, M., Grieser, J., Beck, C., Rudolf, B., Rubel, F., 2006. World map of the Köppen-Geiger climate classification updated. Meteorol. Z. 15 (3), 259–263. https://doi.org/10.1127/0941-2948/2006/0130.
Kunkel, K.E., Easterling, D.R., Kristovich, D.A.R., Gleason, B., Stoecker, L., et al., 2010. Recent Increases in U.S. Heavy Precipitation Associated with Tropical Cyclones. Geophys. Res. Lett. 37, L24706. https://doi.org/10.1029/2010gl045164.
Kunkel, K.E., Frankson, R.M., 2015. Global land surface extremes of precipitation: data limitations and trends. J. Extreme Events 02 (02), 1550004. https://doi.org/10.1142/s2345737615500049.
Li, H., Zhang, Q., Singh, V.P., Shi, P., Sun, P., 2017. Hydrological effects of cropland and climatic changes in Arid and Semi-Arid River Basins: a case study from the Yellow River Basin, China. J. Hydrol. 549, 547–557. https://doi.org/10.1016/j.jhydrol.2017.04.024.
Liu, J., Zhang, Q., Singh, V.P., Shi, P., 2017. Contribution of multiple climatic variables and human activities to streamflow changes across China. J. Hydrol. 545, 145–162. https://doi.org/10.1016/j.jhydrol.2016.12.016.
Livneh, B., Rosenberg, E.A., Lin, C., Nijssen, B., Mishra, V., et al., 2013. A long-term hydrologically based dataset of land surface fluxes and states for the conterminous United States: update and extensions. J. Clim. 26 (23), 9384–9392. https://doi.org/10.1175/jcli-d-12-00508.1.
Miao, Q., 2018. Are we adapting to floods? Evidence from global flooding fatalities. Risk Anal. https://doi.org/10.1111/risa.13245.
Min, S.-K., Zhang, X., Zwiers, F.W., Hegerl, G.C., 2011. Human contribution to more-intense precipitation extremes. Nature 470, 378. https://doi.org/10.1038/nature09763.
Molina, A., Vanacker, V., Brisson, E., Mora, D., Balthazar, V., 2015. Multidecadal change in streamflow associated with anthropogenic disturbances in the tropical Andes. Hydrol. Earth Syst. Sci. 19, 4201–4213. https://doi.org/10.5194/hess-19-4201-2015.
Motta, J.C., Tucci, C.E.M., 1984. Simulation of the urbanization effect in flow. Hydrol. Sci. J. 29 (2), 131–147. https://doi.org/10.1080/02626668409490930.
Nash, J., Sutcliffe, J.V., 1970. River flow forecasting through conceptual models part I—a discussion of principles. J. Hydrol. 10 (3), 282–290. https://doi.org/10.1016/0022-1694(70)90255-6.
National Weather Service, 2018. Accessed in July, 2019 from https://www.weather.gov/ewx/.
National Weather Service, 2019. October 1998 Floods – South Central Texas. Weather Event Summary. Accessed in June, 2019 from https://www.weather.gov/ewx/wxevent-1998flood.
Natsios, A., 2019. Hurricane Harvey: Texas at Risk. Accessed in January, 2019 from http://www.glo.texas.gov/recovery/files/texas-at-risk-report.pdf.
Nauman, R., Dangermond, M., & Frye, C., 2018. United States Department of Agriculture. Soil Survey Geographic (SSURGO) Database for Texas. Retrieved from https://websoilsurvey.nrcs.usda.gov/.
[dataset] NOAA (National Oceanic and Atmospheric Administration). (2019). U.S.

Climate Extremes Index. Web data. Accessed in January, 2019. https://www.ncdc.noaa.gov/extremes/cei/.
Nowak, D.J., Greenfield, E.J., 2012. Tree and impervious cover in the United States. Landscape Urban Plann. 107 (1), 21–30. https://doi.org/10.1016/j.landurbplan.2012.04.005.
Ochoa-Tocachi, B.F., Buytaert, W., De Bièvre, B., 2016. Regionalization of land-use impacts on streamflow using a network of paired catchments. Water Resour. Res. 52 (9), 6710–6729. https://doi.org/10.1002/2016wr018596.
OniStephen, K.F., Martyn, N.B., James, P.H., Dillon, P.J., 2015. Hydrological Footprints of Urban Developments in the Lake Simcoe Watershed, Canada: A Combined Paired-Catchment and Change Detection Modelling Approach. Hydrol. Process. 29 (7), 1829–1843. https://doi.org/10.1002/hyp.10290.
Perkins, W.A., Duan, Z.R., Sun, N., Wigmosta, M.S., Richmond, M.C., et al., 2019. Parallel distributed hydrology soil vegetation model (DHSVM) using global arrays. Environ. Modell. Software 122, 14. https://doi.org/10.1016/j.envsoft.2019.104533.
Peterson, T.C., Folland, C., Gruza, G., Hogg, W., Mokssit, A., et al., 2001. Report of the Activities of the Working Group on Climate Changedetection and Related Rapporteurs.
[dataset] Price, C.V., Nakagaki, N., Hitt, K.J., & Clawges, R.M., 2006. Enhanced Historical Land-Use and Land-Cover Data Sets of the U.S. Geological Survey. Data Series 240. doi:10.3133/ds240. (Accessed in March, 2017).
Putro, B., Kjeldsen, T.R., Hutchins, M.G., Miller, J., 2016. An empirical investigation of climate and land-use effects on water quantity and quality in two urbanising catchments in the southern United Kingdom. Sci. Total Environ. 548–549. https://doi.org/10.1016/j.scitotenv.2015.12.132.
Sankarasubramanian, A., Vogel, R.M., Limbrunner, J.F., 2001. Climate elasticity of streamflow in the United States. Water Resour. Res. 37 (6), 1771–1781.
Schaake, J.C., 1990. From climate to flow. In: Waggoner, P.E. (Ed.), Climate Change and US Water Resources. John Wiley, New York, USA, pp. 177–206.
Schelker, J., Kuglerová, L., Eklöf, K., Bishop, K., Laudon, H., 2013. Hydrological effects of clear-cutting in a boreal forest – snowpack dynamics, snowmelt and streamflow responses. J. Hydrol. 484, 105–114. https://doi.org/10.1016/j.jhydrol.2013.01.015.
Seibert, J., McDonnell, J.J., 2010. Land-cover impacts on streamflow: a change-detection modelling approach that incorporates parameter uncertainty. Hydrol. Sci. J. 55 (3), 316–332. https://doi.org/10.1080/02626661003683264.
Sidibe, M., Dieppois, B., Mahé, G., Paturel, J.-E., Amoussou, E., et al., 2018. Trend and variability in a new, reconstructed streamflow dataset for West and Central Africa, and Climatic Interactions, 1950–2005. J. Hydrol. 561, 478–493. https://doi.org/10.1016/j.jhydrol.2018.04.024.
[dataset] Texas Commission on Environmental Quality. (2017). Water Rights and Water Use Data. Excel file version. Accessed in June, 2017 from https://www.tceq.texas.gov/permitting/water_rights/wr-permitting/wrwud.
[dataset] Thomas, L.M., Nancy, A.P., Enrique, J.L., & Enrique, J.L., 2013. Census 2010 of Population and Housing, Summary Population and Housing Characteristics. U.S. Census Bureau. Retrieved from https://www.census.gov/.
U.S. Geological Survey, 2014. Floods in the Guadalupe and San Antonio River Basins in Texas, October 1998.
U.S. Geological Survey, 2020. Land Change Monitoring, Assessment, and Projection. Accessed in March, 2020 from https://www.usgs.gov/land-resources/eros/lcmap.
United Nations, 2009. Global Assessment Report on Disaster Risk Reduction 2009 – Risk and Poverty in a Changing Climate: Invest Today for a Safer Tomorrow.
United Nations, 2011. Global Assessment Report on Disaster Risk Reduction 2011 – Revealing Risk, Redefining Development. Retrieved from Geneva, Switzerland.
Vogelmann, J.E., Howard, S.M., Yang, L., Larson, C.R., Wylie, B.K., et al., 2001. Completion of the 1990s National Land Cover Data Set for the Conterminous United States from Landsat Thematic Mapper Data and Ancillary Data Sources. Photogramm. Eng. Remote Sens. 67, 652–662.
Wang, Z., Lin, L., Zhang, X., Zhang, H., Liu, L., et al., 2017. Scenario dependence of future changes in climate extremes under 1.5 °C and 2 °C global warming. Sci. Rep. 7, 46432. https://doi.org/10.1038/srep46432.
Westra, S., Alexander, L.V., Zwiers, F.W., 2013. Global increasing trends in annual maximum daily precipitation. J. Clim. 26 (11), 3904–3918. https://doi.org/10.1175/jcli-d-12-00502.1.
White, T., 2018. Record-Setting Flood of 1998 Happened 20 Years Ago This Week in San Antonio Area, South Texas. Accessed in October, 2018 from https://www.mysanantonio.com/news/local/history-culture/article/1998-flooding-san-antonio-south-texas-13314671.php.
Wigmosta, M.S., Vail, L.W., Lettenmaier, D.P., 1994. A distributed hydrology-vegetation model for complex terrain. Water Resour. Res. 30 (6), 1665–1679. https://doi.org/10.1029/94WR00436.
Winters, B.A., Angel, J., Ballerine, C., Byard, J., Flegel, A., et al., 2015. Report for Urban Flooding Awareness Act. Illinois Department of Natural Resources. Accessed in November, 2018 from https://www.dnr.illinois.gov/WaterResources/Documents/Final_UFAA_Report.pdf.
Wood, A.W., Maurer, E.P., Kumar, A., & Lettenmaier, D.P., 2002. Long-Range Experimental Hydrologic Forecasting for the Eastern United States. Journal of Geophysical Research-Atmospheres, 107(D20). doi:10.1029/2001jd000659.
Wood, A.W., Lettenmaier, D.P., 2006. A test bed for new seasonal hydrologic forecasting approaches in the Western United States. Bull. Am. Meteorol. Soc. 87 (12), 1699–1712. https://doi.org/10.1175/bams-87-12-1699.
Yang, L., Smith, J.A., Wright, D.B., Baeck, M.L., Villarini, G., et al., 2013. Urbanization and climate change: an examination of nonstationarities in urban flooding. J. Hydrometeorol. 14 (6), 1791–1809. https://doi.org/10.1175/jhm-d-12-095.1.
Yangon, M., 2016. Water Security and the Sustainable Development Goals (Sdgs). Accessed in October, 2018 from https://www.gwp.org/contentassets/985bec2240b845c6ae9ea08446fcbd22/myanmar—high-level-round-table-final-report.pdf.
Zarezadeh, V., Giacomoni, M., 2017. Incorporating dynamic land use change into hydrologic model to assess urbanization effects on hydrologic flow regime. World Environ. Water Resour. Congress 22–32. https://doi.org/10.1061/9780784480601.003.
Zégre, N., Skaugset, A.E., Som, N.A., McDonnell, J.J., Ganio, L.M., 2010. In Lieu of the Paired Catchment Approach: Hydrologic Model Change Detection at the Catchment Scale. Water Resour. Res. 46 (W11544). https://doi.org/10.1029/2009wr008601.
Zhang, X., Alexander, L., Hegerl, G.C., Jones, P., Tank, A.K., et al., 2011. Indices for monitoring changes in extremes based on daily temperature and precipitation data. WIRESClimate Change 2 (6), 851–870. https://doi.org/10.1002/wcc.147.
Zhao, G., Gao, H., Cuo, L., 2016a. Effects of urbanization and climate change on peak flows over the San Antonio River Basin, Texas. J. Hydrometeorol. 17 (9), 2371–2389. https://doi.org/10.1175/JHM-D-15-0216.1.
Zhao, G., Gao, H., Naz, B., Kao, S.-C., Voisin, N., 2016b. Integrating a reservoir regulation scheme into a spatially distributed hydrological model. Adv. Water Resour. 98, 16–31. https://doi.org/10.1016/j.advwatres.2016.10.014.
Zhao, G., Gao, H., Kao, S.-C., Voisin, N., Naz, B.S., 2018. A modeling framework for evaluating the drought resilience of a surface water supply system under non-stationarity. J. Hydrol. 563, 22–32. https://doi.org/10.1016/j.jhydrol.2018.05.037.
Zhao, M., Zeng, C., Liu, Z., Wang, S., 2010. Effect of Different Land Use/Land Cover on Karst Hydrogeochemistry: A Paired Catchment Study of Chenqi and Dengzhanhe, Puding, Guizhou, Sw China. J. Hydrol. 388 (1–2), 121–130. https://doi.org/10.1016/j.jhydrol.2010.04.034.
Zhao, F., Zhang, L., Xu, Z., Scott, D.F., 2010a. Evaluation of methods for estimating the effects of vegetation change and climate variability on streamflow. Water Resour. Res. 46 (3). https://doi.org/10.1029/2009wr007702.
Zhu, Z., Woodcock, C.E., 2014. Continuous change detection and classification of land cover using all available landsat data. Remote Sens. Environ. 144, 152–171. https://doi.org/10.1016/j.rse.2014.01.011.